Journal of Signal Processing Systems
https://doi.org/10.1007/s11265-021-01667-x

Machine Learning Detects Distinct Subtypes of Minimal Cognitive Impairment

Rong Chen[1] · Edward H. Herskovits[1] · for the Alzheimer's Disease Neuroimaging Initiative

Received: 31 July 2020 / Revised: 17 March 2021 / Accepted: 21 April 2021

Abstract
Minimal cognitive impairment (MCI), a potential precursor to Alzheimer's disease (AD), may be a heterogeneous entity consisting of distinct subtypes. To evaluate this hypothesis, we applied unsupervised machine-learning to a subset of the Alzheimer's disease Neuroimaging Initiative (ADNI) data set, and detected MCI subtypes with distinct clinical correlates. Our subtype-detection system consists of preprocessing, clustering, validation, and visualization modules. We applied this system to data from MCI subjects in the ADNI-2 cohort. The resulting six subtypes demonstrated different profiles with respect to cognitive and laboratory assessment, potentially indicating differing clinical trajectories and treatment responses.

Keywords Machine learning · Neuroinformatics · Alzheimer's disease · Minimal cognitive impairment

1 Introduction

Identifying and diagnosing diseases based on history and physical examination is a practice that predates Hippocrates. As non-observational biomarkers of disease, such as temperature and blood pressure measurement, clinical and anatomic pathology laboratory tests, and radiologic examinations, have become available, biomedical researchers have used these data to characterize subtypes of disease categories such as infection and cancer; we refer to this process as subtype detection. Researchers and clinicians have characterized subtypes by noticing differences among patients thought to have the same disorder. For example, patients presenting with skin lesions may experience no adverse outcomes, or may go on to develop disseminated disease; histological analysis of these lesions identifies biomarkers (e.g., atypical mitoses) that are associated with these outcome subtypes.

Neuropsychiatric disorders, such as schizophrenia, have historically been classified based on clinical symptoms and signs [1], as laboratory tests have not been found to be prognostically useful for some disorders. Although clinical scales have been employed to diagnose and characterize Parkinson's disease [2] and Alzheimer's disease [3], some of the clinical features that underpin the diagnosis of neuropsychiatric disorders may be subjective. The advent of noninvasive methods for interrogating brain structure and connectivity, such as T1-weighted magnetic-resonance imaging (MRI), diffusion tensor imaging (DTI) and resting-state functional magnetic-resonance imaging (rs-fMRI), promise objective biomarkers for characterizing neuropsychiatric disorders, notwithstanding problems related to reproducibility across sites and equipment manufacturers. Similarly, the advent of inexpensive, noninvasive genomic interrogation, including whole-genome sequencing [4] and microarray analysis of gene expression [5, 6] enable researchers to evaluate the genetic contributions to neuropsychiatric disorders.

In addition to reproducibility, one of the factors limiting characterization of neuropsychiatric disorders based on clinical, connectivity, and genetic biomarkers is the immense

Data used in preparation of this article were obtained from the Alzheimer's Disease Neuroimaging Initiative (ADNI) database (adni.loni.usc.edu). As such, the investigators within the ADNI contributed to the design and implementation of ADNI and/or provided data but did not participate in analysis or writing of this report. A complete listing of ADNI investigators can be found at: http://adni.loni.usc.edu/wp-content/uploads/how_to_apply/ADNI_Acknowledgement_List.pdf.

✉ Edward H. Herskovits
eherskovits@som.umaryland.edu

Rong Chen
rchen@som.umaryland.edu

[1] Department of Diagnostic Radiology and Nuclear Medicine, The University of Maryland School of Medicine, 22 S Greene Street, Baltimore, MD 21201, USA

Published online: 16 June 2021

numbers of image and genetic variables from which biomedical researchers would select those that identify a distinct clinical entity. Recent advances in data science and computer hardware have greatly extended the utility of computational approaches to subtype detection. The task of identifying novel subgroups in a data set is an unsupervised machine-learning problem; that is, the data provided to the machine-learning algorithm do not include the group to which each individual (or sample) belongs [7]. Our hypothesis is that unsupervised machine learning can derive useful subgroups from large, complex biomedical data sets. We test this hypothesis in the domain of minimal cognitive impairment (MCI), by designing and implementing a platform for the automated subtype detection based on T1-weighted MRI and positron-emission tomography (PET) image data, and for validation of these subtypes based on clinical and model-performance features.

2 Methods

We developed a machine-learning system to detect subtypes based on multimodal biomarkers. The proposed system has four major components: preprocessing, clustering, validation, and visualization. The preprocessing module includes operations required before machine-learning algorithms can be applied to the data. For example, for multimodal image data such as T1-weighted MRI, DTI, rs-fMRI, and PET, preprocessing might include registration to a common coordinate space, skull stripping, intensity correction, and segmentation, to generate image-derived features. Additional operations, such as normalization to 0 mean and unit variance, also occur during preprocessing. The clustering module groups subjects into subtypes. The validation module associates the generated subtypes with variables not used for clustering, such as clinical assessment scales. The visualization module depicts the results to facilitate the characterization of subtypes. Each module is extensible. For example, we can extend the clustering module to include deep learning based clustering algorithms.

The proposed system is based on R and Python, which are freely available; it does not depend on proprietary third-party libraries. The proposed system is cross-platform and supports Windows, Mac OS, and Unix/Linux.

2.1 Subjects

We obtained the data used in the preparation of this manuscript from the ADNI database (adni.loni.usc.edu), Principal Investigator Michael W. Weiner, MD. For additional information about ADNI, visit www.adni-info.org. We limited this analysis to the ADNI-2 [8] cohort, and in particular to those subjects with MCI. In addition, we used data from ADNI-2 normal control subjects during preprocessing only, as described below.

2.2 MRI-Derived Features

We analyzed the baseline T1-weighted MRI data acquired from MCI subjects in the ADNI-2 [8] data set. We included volumes of the hippocampus, entorhinal cortex, fusiform gyrus, medial temporal lobe, whole brain, ventricle, and intracranial volume, generated by the UCSF pipeline; we downloaded these data from the ADNI website. As these processed values are available to download, we did not invoke our image-preprocessing pipeline.

2.3 PET-Derived Features

Researchers have found that fluoro-deoxy glucose (FDG) [9] and Florbetapir (AV-45) [9, 10] PET standardized uptake values (SUVs) are associated with MCI and Alzheimer's disease status and progression. We therefore included the AV-45 standardized uptake value ratio (SUVR) averaged across frontal cortex, anterior cingulate, precuneus cortex, and parietal cortex, relative to the cerebellum; and average FDG-PET SUVs for angular, temporal, and posterior cingulate regions. Note that ADNI-2 combines left- and right-sided structures, such as ventricles and brain regions, into a single structure. These data were downloaded from the ADNI website. As with the MRI-derived variables, these processed PET-derived values are available to download, so we did not invoke our image-preprocessing pipeline.

2.4 Preprocessing

As described above, since this data set includes structure-wise structural MRI and PET SUV data, rather than unprocessed image data, there was no need to preprocess images for this analysis. Similar to the procedure described in [11], we preprocessed the quantitative MRI volumetric and PET SUV data by removing zero-variance variables and variables that didn't significantly differ between controls and MCI subjects; regressing out age and sex effects from the remaining variables; and then scaling to 0 mean and unit variance.

2.5 Unsupervised Machine Learning

To detect MCI subtypes, we employed the unsupervised machine-learning framework described in [11], which is based on clustering. Clustering is defined as the problem of partitioning objects into clusters (groups). Objects in the same cluster are similar, whereas objects in different clusters are dissimilar. An important problem in clustering is to determine the number of clusters. We employed Affinity Propagation Clustering (APC) [12], in particular the apcluster package in R, to estimate the number of clusters. We then provided the number of clusters to the BIRCH clustering algorithm [13], in particular the sklearn.cluster package in Python, to detect MCI

subtypes based on these image-derived variables. We used the BIRCH algorithm for clustering because it's a memory-efficient, online-learning algorithm. The BIRCH algorithm constructs a balanced tree of Clustering Features (CFs) based on the cluster centroids. A CF is a data structure that represents a cluster by storing the number of elements, their linear sum, and their squared sum. For a new object, BIRCH descends the tree by following its closest CF until a leaf node is reached. The new object is either merged into its closest leaf-CF or inserted as a new leaf.

2.6 Validation

To determine clinical correlates of subtypes derived from machine learning, we evaluated associations among MCI subtypes and clinical assessment, genetic variables, and clinical-laboratory values, based on effect size. For a continuous variable, we computed one-way ANOVA statistics, and η^2 as the measure of effect size. For categorical variables, we computed chi-squared statistics, and Cramer's phi as the measure of effect size.

2.7 Visualization

We used principal component analysis (PCA) to project raw data onto a 2D space in order to visualize the detected subtypes, where the x-axis is the first principal component and the y-axis is the second principal component. We also plotted the profiles of the input image-derived variables in a heatmap. In this heatmap, each element is the average intensity of the variable across all subjects in a cluster; rows are variables and columns are subtypes.

3 Results

3.1 Subtypes

We removed whole-brain and intracranial volumes from analysis because they didn't differ across control and MCI groups. Our final feature set included 7 variables: volumes of the hippocampus (Hippocampus), entorhinal cortex (Entorhinal), fusiform gyrus (Fusiform), medial temporal lobe (MedTemp), and ventricles (Ventricle); average FDG-PET (FDG) of angular, temporal, and posterior cingulate gyri, and AV-45 SUVR (AV-45) averaged across frontal cortex, anterior cingulate, precuneus cortex, and parietal cortex, relative to the cerebellum. Of the 469 ADNI-2 MCI subjects, 360 had no missing data for these variables. We used data from 294 ADNI-2 control subjects only to eliminate variables for which there was no difference between controls and MCI subjects, as described in Section 2.4.

Unsupervised machine learning detected six MCI subtypes (n = 33, 76, 28, 154, 30, and 39, respectively), which were well separated by the first two principal components (Fig. 1). All image-derived features demonstrated differential patterns across subtypes. In Fig. 1, we ranked features by effect size (η^2); ventricular and hippocampal volumes had the largest effect sizes. The heatmap in Fig. 1 indicates that subtype 3 is based primarily on atrophy (i.e., low cortical volumes and high ventricular volumes), low FDG SUV (i.e., low cortical glucose metabolism), and intermediate AV-45 SUVR. Subtype 6 is similar to subtype 3, except for higher AV-45 and lower ventricular volumes. Subtype 5 is characterized by relatively high cortical volumes and FDG SUV, and low AV-45 SUVR and ventricular volume. Subtypes 1, 2 and 4 are characterized by intermediate cortical volume, but differ with respect to AV-45 (high in subtype 2), ventricular volumes (greater in subtype 1 than in any other subtype) and, to a lesser extent, with respect to FDG SUV (slightly higher in subtype 4).

3.2 Validation

To determine the potential clinical relevance of our MCI subtypes, we analyzed subtype associations with the following clinical assessments: the 11-item version of the Alzheimer's Disease Assessment Scale–Cognitive subscale (ADAS11; higher score is worse) [14]; ADAS13 (higher is worse) is an extension of ADAS11 with additional delayed recall and digit cancellation tasks; ADNI modified Preclinical Alzheimer's Cognitive Composite (PACC) [15] with Digit Symbol Substitution (PACC_digit; lower is worse); ADNI modified Preclinical Alzheimer's Cognitive Composite (PACC) with Trials B (PACC_trials_b; lower is worse); the Rey Auditory Verbal Learning Test Learning [16] Percent Forgetting (RAVLT_perc_forgetting; higher is worse); and the Rey Auditory Verbal Learning Test Immediate (RAVLT_immediate; lower is worse).

We found that MCI subtype is significantly associated with these clinical variables (Table 1). In particular, subtypes 3 and 6, which have image-derived profiles indicative of atrophy and increased amyloid deposition, also have relatively increased ADAS11 and ADAS13 scores, which indicate problems with recall; lower PACC scores, which are indicative of relative cognitive decline; relatively high RAVLT percent forgetting and relatively low RAVLT immediate recall, which are indicative of impaired short-term memory. In contrast, subtype 5, which has an image-derived profile indicative of normal brain volumes and metabolism, had the lowest average ADAS11 and ADAS13 scores, the second lowest RAVLT percent forgetting score, and the highest PACC and second-highest RAVLT immediate-recall scores.

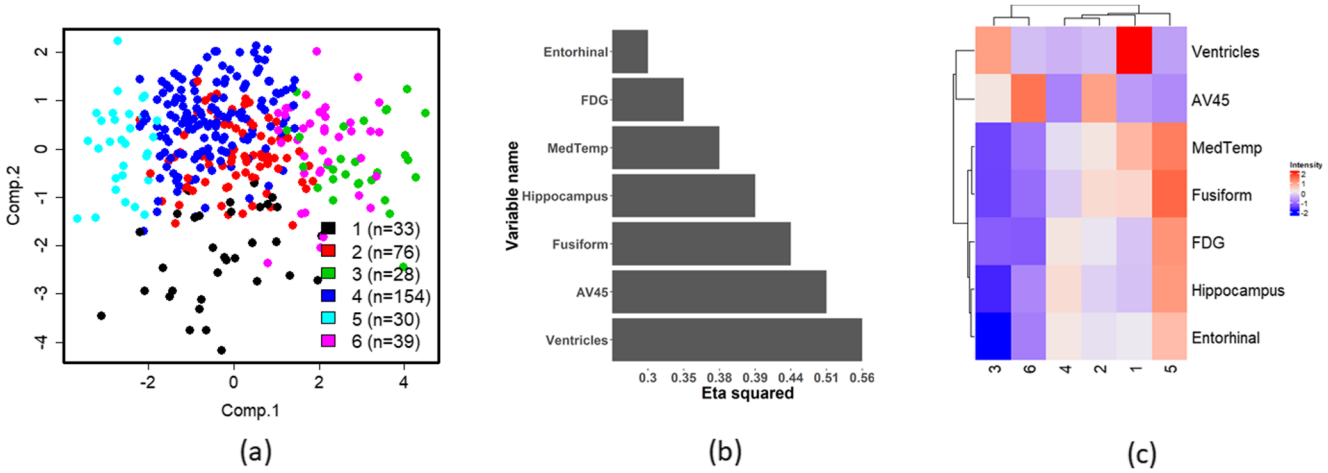

Figure 1 Image-derived subtype detection results for the ADNI-2 data set. **a** Principal component analysis (PCA) plot of MCA subtypes. Component 1 and Component 2 are the first and second principal components, respectively. **b** Variable importance, ranked by effect size (η^2). **c** Neuroimaging variable profiles displayed as a heatmap across MCI subtypes.

Figure 2 further elucidates MCI subtype differences. Subtypes 3 and 6 differ significantly from the other subtypes with respect to functional measures ADAS11 and ADAS13. With respect to PACC_digit and PACC_trials_b, there appear to be 3 groups, consisting of subtypes 3 and 6 (low scores), 1 and 2 (intermediate scores), and 4 and 5 (high scores). Subtype 4 manifested lower RAVLT_perc_forgetting than most other subtypes, whereas subtypes 3 and 6 manifested modestly increased RAVLT_perc_forgetting scores. Subtype 4 exceeded most other subtypes with respect to RAVLT_immediate.

The Apolipoprotein E (APOE) gene is polymorphic, with three major isoforms: ε2, ε3, and ε4. Two APOE ε4 alleles confer high risk, one APOE ε4 allele confers intermediate risk, and zero alleles indicate relatively low risk of developing AD [17]. In the ADNI-2 cohort, APOE status is indicated as zero, one, or two APOE ε4 alleles. We found that image-derived MCI subtype is significantly associated with APOE status (chi-square $p < 0.0001$). As shown in Fig. 3, subtype 6 has the highest proportion of subjects with one or two APOE ε4 alleles, whereas subtypes 1, 4, and 5 have relatively low proportions of subjects with one or two ε4 alleles. MCI subtypes 2 and 3 would have intermediate AD risk based on APOE status. Again, these results are concordant with image-derived features for the subtypes (Fig. 1).

3.3 Laboratory-Test Validation

Cerebrospinal fluid levels of β-amyloid, total-tau, and phosphor-tau differed across subtypes (Fig. 4a-c, ANOVA $p < 0.0001$, < 0.0001, $= 0.0001$, respectively). The profile of subtype 6 differs most from the others: using the mean across all groups (dashed horizontal line) as the reference, MCI subtype 6 has relatively high β-amyloid, tau, total-tau, and phosphor-tau.

Table 1 Associations between MCI subtypes 1–6 and clinical variables, reported as mean ± standard deviation, and ANOVA p-value.

	MCI Subtype						
Clinical Variable	1	2	3	4	5	6	P-value
ADAS11	10.27±4.79	9.70±4.08	13.04±5.07	7.45±3.13	6.60±3.09	11.51±4.27	<0.001
ASAS13	15.88±6.43	15.92±6.07	20.57±6.45	11.75±4.93	10.50±4.37	19.26±6.28	<0.001
PACC_digit	-5.76±3.32	-5.96±3.67	-8.14±4.41	-3.46±3.20	-3.31±2.91	-8.74±4.50	<0.001
PACC_trials_b	-4.80±3.01	-4.99±3.19	-6.98±3.60	-2.86±2.89	-2.64±2.59	-7.63±3.65	<0.001
RAVLT_perc_forgetting	5.09±2.10	4.91±2.33	5.71±2.59	3.97±2.56	4.07±2.27	5.51±2.47	<0.001
RAVLT_immediate	34.79±10.27	34.16±8.91	30.25±8.36	41.70±11.24	37.97±9.87	32.82±8.53	<0.001

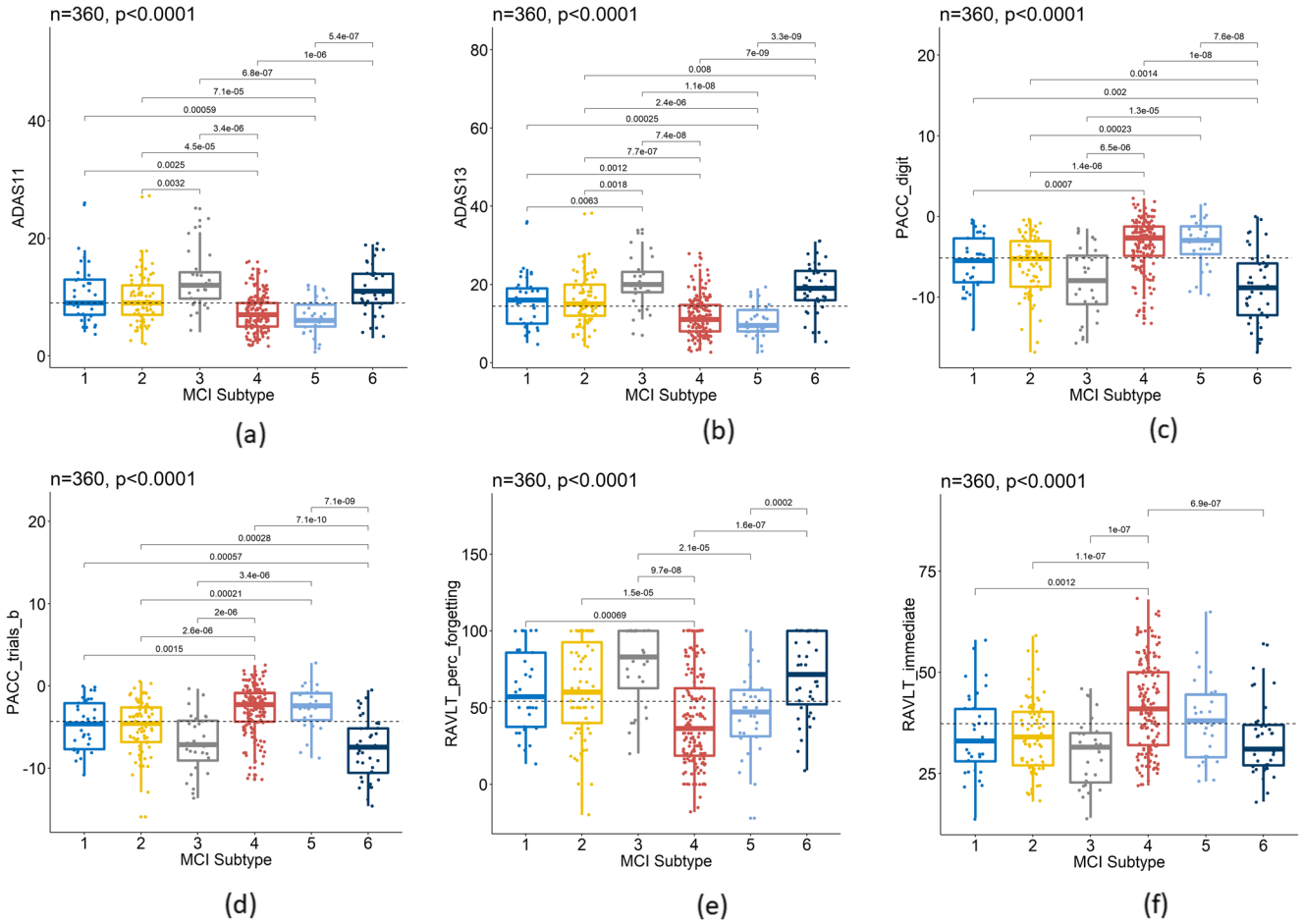

Figure 2 Associations between MCI subtype and functional clinical assessments; see text for assessment details.

4 Discussion

Neuropsychiatric disorders have historically been demarcated by symptoms and signs. We have demonstrated that unsupervised machine learning can be applied to image-derived biomarkers from the ADNI-2 cohort to detect MCI subtypes with distinct clinical features, including cognitive-test results, genetic profile, and clinical-laboratory values. Of note, validation results for the subtypes we detected are concordant across clinical, laboratory and genetic results, indicating that the subtypes are clinically valid, rather than statistical artifacts.

With respect to MCI, to our knowledge there is no previous peer-reviewed report describing the application of unsupervised machine learning to derive MCI subtypes. The literature indicates that subtypes have been assigned based on clinical criteria [18–20]. However, supervised machine learning has been applied extensively to assign patients to clinically established MCI subtypes [21–23].

Limitations of this analysis include restriction to a relatively small number of biomarkers, and lack of a simple method for summarizing subgroup differences. We plan to greatly extend this analysis to include DTI and genetic data as indicators (in which case the latter would not be used for

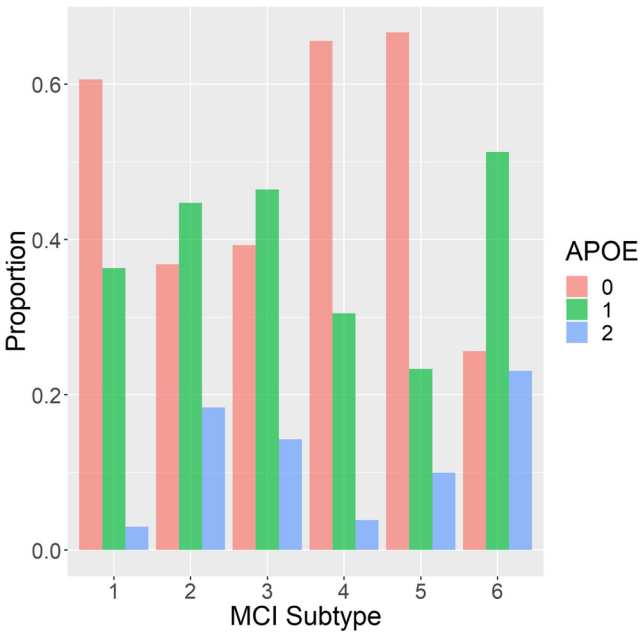

Figure 3 Histograms of APOE status (number of ε4 alleles) across MCI subtypes.

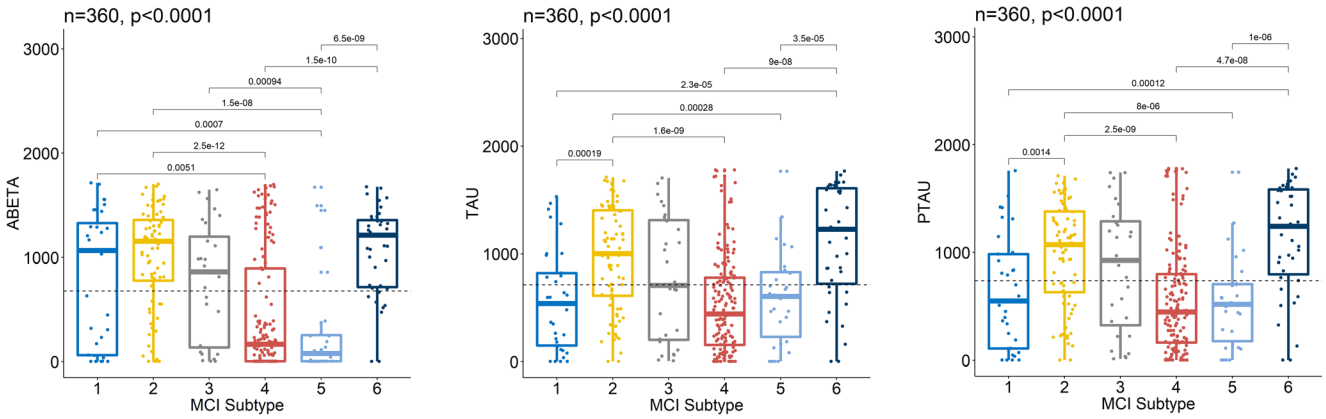

Figure 4 Associations between MCI subtype and cerebrospinal fluid levels of β-amyloid (left), total-tau (middle), and phosphor-tau (right). The dashed horizontal line is the mean across all 360 MCI subjects.

validation). In addition, we will extend validation to include models derived from supervised learning; to the extent that cross validation of these models indicates high classification accuracy, those results would indicate valid—i.e., separable—subtypes. Ultimately, before applying subtypes derived from machine learning to foster precision medicine, researchers must validate these subtypes in clinical trials.

Our subtype-detection framework is modular, and is therefore easily extended. For example, we could add t-Distributed Stochastic Neighbor Embedding [24] to the visualization module for visualizing high-dimensional data. Furthermore, we have already implemented several clustering methods, in addition to BIRCH [11]. For multimodal neuroimaging data, we can use joint embedding to extract latent variables that represent shared information across different modalities, and then perform clustering based on the latent-variable representation.

Data collection and sharing for this project was funded by the ADNI (NIH U01 AG024904; Department of Defense W81XWH-12-2-0012). ADNI is funded by the National Institute on Aging, the National Institute of Biomedical Imaging and Bioengineering, and through generous contributions from the following: AbbVie, Alzheimer's Association; Alzheimer's Drug Discovery Foundation; Araclon Biotech; BioClinica, Inc.; Biogen; Bristol-Myers Squibb Company; CereSpir, Inc.; Cogstate; Eisai Inc.; Elan Pharmaceuticals, Inc.; Eli Lilly and Company; EuroImmun; F. Hoffmann-La Roche Ltd and its affiliated company Genentech, Inc.; Fujirebio; GE Healthcare; IXICO Ltd.; Janssen Alzheimer Immunotherapy Research & Development, LLC.; Johnson & Johnson Pharmaceutical Research & Development LLC.; Lumosity; Lundbeck; Merck & Co., Inc.; Meso Scale Diagnostics, LLC.; NeuroRx Research; Neurotrack Technologies; Novartis Pharmaceuticals Corporation; Pfizer Inc.; Piramal Imaging; Servier; Takeda Pharmaceutical Company; and Transition Therapeutics. The Canadian Institutes of Health Research is providing funds to support ADNI clinical sites in Canada.

Acknowledgements This work was supported by the NIH NINDS R01-NS110421 and the BRAIN Initiative, NIA R21-AG058118, and NINDS R21-NS108811.

References

1. American Psychiatric Association. (2013). *Diagnostic and Statistical Manual of Mental Disorders* (5th edition.). American Psychiatric Association. https://doi.org/10.1176/appi.books.9780890425596.
2. Goetz, C. G., Fahn, S., Martinez-Martin, P., Poewe, W., Sampaio, C., Stebbins, G. T., … LaPelle, N. (2007). Movement Disorder Society-sponsored revision of the Unified Parkinson's Disease Rating Scale (MDS-UPDRS): Process, format, and clinimetric testing plan. *Movement Disorders, 22*(1), 41–47. https://doi.org/10.1002/mds.21198.
3. Mohs, R. C., & Cohen, L. (1988). Alzheimer's disease assessment scale (ADAS). *Psychopharmacol Bull, 24*(4), 627–628.
4. Ng, P. C., & Kirkness, E. F. (2010). Whole genome sequencing. In M. R. Barnes & G. Breen (Eds.), *Genetic Variation: Methods and Protocols* (pp. 215–226). Humana Press. https://doi.org/10.1007/978-1-60327-367-1_12.
5. Duggan, D. J., Bittner, M., Chen, Y., Meltzer, P., & Trent, J. M. (1999). Expression profiling using cDNA microarrays. *Nature Genetics, 21*(1), 10–14. https://doi.org/10.1038/4434.
6. Taub, F. E., DeLeo, J. M., & Thompson, E. B. (1983). Sequential comparative hybridizations analyzed by computerized image processing can identify and quantitate regulated RNAs. *DNA (Mary Ann Liebert, Inc.), 2*(4), 309–327. https://doi.org/10.1089/dna.1983.2.309.
7. Duda, R. O., Hart, P. E., & Stork, D. G. (2000). *Pattern Classification* (2nd Edition). Wiley-Interscience.
8. Beckett, L. A., Donohue, M. C., Wang, C., Aisen, P., Harvey, D. J., Saito, N., & Alzheimer's Disease Neuroimaging Initiative. (2015). The Alzheimer's disease neuroimaging initiative phase 2: Increasing the length, breadth, and depth of our understanding. *Alzheimer's & Dementia, 11*(7), 823–831. https://doi.org/10.1016/j.jalz.2015.05.004.
9. Johnson, K. A., Sperling, R. A., Gidicsin, C.M., Carmasin, J. S., Maye, J. E., Coleman, R. E., … Skovronsky, D. M. (2013).Florbetapir (F18-AV-45) PET to assess amyloid burden in Alzheimer's diseasedementia, mild cognitive impairment, and normal aging. *Alzheimer's & Dementia*, *9*(5, Supplement), S72–S83. https://doi.org/10.1016/j.jalz.2012.10.007.

10. Wong, D. F., Rosenberg, P. B., Zhou, Y., Kumar,A., Raymont, V., Ravert, H. T., … Pontecorvo, M. J. (2010). In vivo imaging of amyloid deposition in Alzheimer disease using the radioligand 18F-AV-45(Flobetapir F 18). *Journal of Nuclear Medicine*, *51*(6), 913–920. https://doi.org/10.2967/jnumed.109.069088.
11. Chen, R., Lee, K., & Herskovits, E. H. (2020). Computational framework for detection of subtypes of neuropsychiatric disorders based on DTI-derived anatomical connectivity. *The Neuroradiology Journal*. https://doi.org/10.1177/1971400920950694.
12. Frey, B. J., & Dueck, D. (2007). Clustering by passing messages between data points. *Science, 315*(5814), 972–976. https://doi.org/10.1126/science.1136800.
13. Zhang, T., Ramakrishnan, R., & Livny, M. (1997). BIRCH: A new data clustering algorithm and its applications. *Data Mining and Knowledge Discovery, 1*(2), 141–182. https://doi.org/10.1023/A:1009783824328.
14. Rosen, W. G., Mohs, R. C., & Davis, K. L. (1984). A new rating scale for Alzheimer's disease. *The American Journal of Psychiatry, 141*(11), 1356–1364. https://doi.org/10.1176/ajp.141.11.1356.
15. Donohue, M. C., Sperling, R. A., Salmon, D. P.,Rentz, D. M., Raman, R., Thomas, R. G., … Aisen, P. S. (2014). The preclinical Alzheimer cognitive composite: measuring amyloid-related decline. *JAMA Neurology*, *71*(8), 961–970. https://doi.org/10.1001/jamaneurol.2014.803.
16. Estévez-González, A., Kulisevsky, J., Boltes, A., Otermín, P., & García-Sánchez, C. (2003). Rey verbal learning test is a useful tool for differential diagnosis in the preclinical phase of Alzheimer's disease: comparison with mild cognitive impairment and normal aging. *International Journal of Geriatric Psychiatry, 18*(11), 1021–1028. https://doi.org/10.1002/gps.1010.
17. Sando, S. B., Melquist, S., Cannon, A., Hutton,M. L., Sletvold, O., Saltvedt, I., … Aasly, J. O. (2008). APOE ε4 lowers age at onset and is a high risk factor for Alzheimer's disease; A case control study from central Norway. *BMC Neurology*, *8*, 9. https://doi.org/10.1186/1471-2377-8-9.
18. Rapp, S. R., Legault, C., Henderson, V. W.,Brunner, R. L., Masaki, K., Jones, B., … Thal, L. (2010). Subtypes of mild cognitive impairment in older postmenopausal women: the women's health initiative memory study. *Alzheimer disease and associated disorders*, *24*(3), 248–255. https://doi.org/10.1097/WAD.0b013e3181d715d5.
19. Trittschuh,E. H., Crane, P. K., Larson, E. B., Cholerton, B., McCormick, W. C., McCurry,S. M., … Craft, S. (2011). Effects of varying diagnostic criteria on prevalence of mild cognitive impairment in a community based sample. *Journal of Alzheimer's Disease: JAD*, *25*(1), 163–173. https://doi.org/10.3233/JAD-2011-101821.
20. Whitwell, J. L., Petersen, R. C., Negash, S.,Weigand, S. D., Kantarci, K., Ivnik, R. J., … Jack, C. R. (2007). Patterns of atrophy differ among specific subtypes of mild cognitive impairment. *Archives of Neurology*, *64*(8), 1130. https://doi.org/10.1001/archneur.64.8.1130.
21. Haller, S., Missonnier, P., Herrmann, F. R.,Rodriguez, C., Deiber, M.-P., Nguyen, D., … Giannakopoulos, P. (2013). Individualclassification of mild cognitive impairment subtypes by support vector machineanalysis of white matter DTI. *AJNR. American journal of neuroradiology*, *34*(2), 283–291. https://doi.org/10.3174/ajnr.A3223.
22. Binaco, R., Calzaretto, N., Epifano, J.,McGuire, S., Umer, M., Emrani, S., … Polikar, R. (2020). Machine learning analysis of digital clock drawing test performance for differential classification of mild cognitive impairment subtypes versus Alzheimer's disease. *Journal of the International Neuropsychological Society: JINS*, *26*(7), 690–700. https://doi.org/10.1017/S1355617720000144.
23. Guan, H., Liu, T., Jiang, J., Tao, D., Zhang,J., Niu, H., … Wen, W. (2017). Classifying MCI subtypes in community-dwelling elderly using cross-sectional and longitudinal MRI-based biomarkers. *Frontiers in Aging Neuroscience*, *9*. https://doi.org/10.3389/fnagi.2017.00309.
24. van der Maaten, L., & Hinton, G. (2008). Visualizing data using t-SNE. *Journal of machine learning research, 9*(Nov), 2579–2605.